

# Atlas Fusion - Modern Framework for Autonomous Agent Sensor Data Fusion

Adam Ligocki<sup>1</sup>, Ales Jelinek<sup>1</sup> and Ludek Zalud<sup>1</sup>

**Abstract**—In this paper, we present our new sensor fusion framework for self-driving cars and other autonomous robots. We have designed our framework as a universal and scalable platform for building up a robust 3D model of the agent’s surrounding environment by fusing a wide range of various sensors into the data model that we can use as a basement for the decision making and planning algorithms. Our software currently covers the data fusion of the RGB and thermal cameras, 3D LiDARs, 3D IMU, and a GNSS positioning. The framework covers a complete pipeline from data loading, filtering, preprocessing, environment model construction, visualization, and data storage. The architecture allows the community to modify the existing setup or to extend our solution with new ideas. The entire software is fully compatible with ROS (Robotic Operation System), which allows the framework to cooperate with other ROS-based software. The source codes are fully available as an open-source under the MIT license. See <https://github.com/Robotics-BUT/Atlas-Fusion>.

## I. INTRODUCTION

As the world is diving deeper into the problem of self-driving cars and other autonomous robots, there is a large number of sophisticated systems for analyzing data and controlling the specific problems of autonomous behaviour. However, these systems, like [1] or [2] are very complex and require dozens of hours to understand the architecture and to be able to start to develop a new solution on top of the existing one.

As members of the academic community, we are experimenting with many new approaches, and our primary motivation is to search for new ways, how to improve the current state of the art techniques. For this purpose, we have designed a system that is aiming at surrounding environment sensing and map building in mobile robotics.

As a result of the AutoDrive research project <https://autodrive-project.eu>, our team has created this

The work has been performed in the project NewControl: Integrated, Fail-Operational, Cognitive Perception, Planning and Control Systems for Highly Automated Vehicles, under grant agreement No 826653/8A19006 and partially in AutoDrive project, under grant agreement 737469. The work was co-funded by grants of Ministry of Education, Youth and Sports of the Czech Republic and Electronic Component Systems for European Leadership Joint Undertaking (ECSEL JU). The work was supported by the infrastructure of RICAIP that has received funding from the European Union’s Horizon 2020 research and innovation programme under grant agreement No 857306 and from Ministry of Education, Youth and Sports under OP RDE grant agreement No CZ.02.1.01/0.0/0.0/17.043/0010085.

<sup>1</sup>All the authors are with the Central European Institute of Technology (CEITEC), Cybernetics in Material Science research group, Brno University of Technology, Purkynova 123, Brno-Kralovo Pole, Czechia, [adam.ligocki@ceitec.vutbr.cz](mailto:adam.ligocki@ceitec.vutbr.cz), [ales.jelinek@ceitec.vutbr.cz](mailto:ales.jelinek@ceitec.vutbr.cz), [ludek.zalud@ceitec.vutbr.cz](mailto:ludek.zalud@ceitec.vutbr.cz)

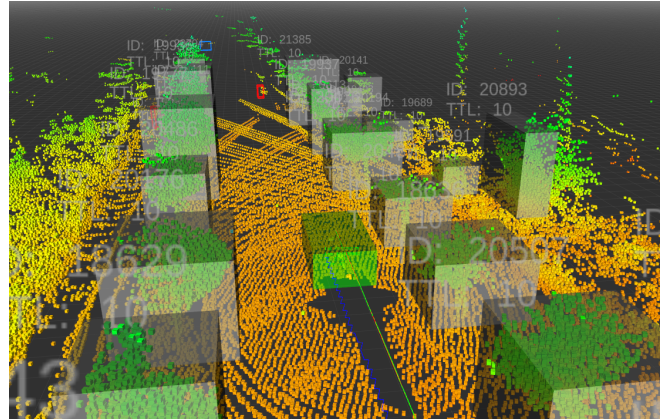


Fig. 1. RViz visualization of the runtime model of the surrounding environment. Grey boxes are the LiDAR-based detections, and color frustums are the neural network detections on the RGB images. The green object at the center is a representation of the agent and the lines behind the agent are the trajectories estimated by different filtering algorithms.

C++ framework that is focusing on data fusion from the various sensor types into a robust representation of the robot’s surroundings model. This model of the environment could provide useful information for the planning and decision-making algorithms in the later phase of the agent’s pipeline.

It is crucial to mention at the very beginning that we have not created this framework with the idea of high performance, high concurrency, and a multi-threading system. We have been focusing on clear architecture, easy scalability, and simple pipeline modification. Our primary purpose was to create a platform for fast prototyping and testing of the mapping algorithms. Because of this, we have decided to design this software as a single thread, blocking pipeline, which is easy to debug, and the outputs are deterministic.

## II. GENERAL ARCHITECTURE DESCRIPTION

We have designed the software with the idea of a very minimalistic pipeline and simple modification so that we can very quickly develop and deploy new ideas and algorithms. Because of this, we have proposed an architecture that separates modules into the independent entities so anybody can easily add the new blocks or bypass or completely turn off the existing ones.

### A. Input Data

As an input data format, we have chosen the same representation that has been used previously in our work on Brno Urban Dataset [3], which is inspired by [4]. The repository contains over ten hours of the real-live traffic situations

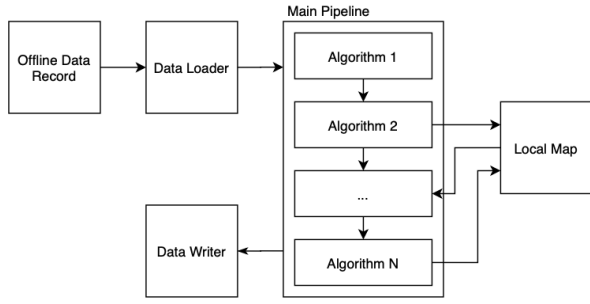


Fig. 2. Schematic, which describes the general structure of the framework. The Data Loader passes the offline loaded data to the main pipeline, which linearly aggregates all the mapping algorithms. Local Map module aggregates and fuses all the outputs of the mapping process. Some type of mapping data is also useful for other purposes, line neural network learning. These data are stored back on disk by the Data Writer module.

that cover city center, highways, suburbs, and countryside environments.

The data are stored as an h265 video in case of RGB and thermal camera data, .ply files for LiDAR scans, and CSV data files for GNSS, IMU, and camera and LiDAR timestamps.

The details of the data loading are described in the III-A subsection below.

### B. Core Pipeline

At the startup, the program reads the basic configuration from the config file (see II-D). The configuration provides a path to the offline record, and the data loading module loads up all the necessary information for offline data interpreting. After that, the main pipeline begins.

The data loading module loader all time-ordered timestamps into the memory and the module later provides data in the correct time order, one by one. Based on the data type (which sensor does the data come from), the pipeline redirects data into the dedicated processing section. The output data, like detected obstacles, static obstacles, or moving entities, are stored in the local map data model.

The entire pipeline has a linear architecture, so the data processing algorithms are sorted one by one. This waterfall-like design allows anybody to add or remove a new data processing algorithm without affecting the current ones.

For every output data model, there is a fully traceable origin, which means that every data model has a reference to the input data which it comes from.

Currently, our system does not provide the possibility of live data processing but plan to add this feature in the future.

### C. Outputs

Generally speaking, the main output of the framework is the map of the surroundings, stored in the Local Map block, with the precise detection of the possible static and dynamic obstacles. The following decision-making algorithms can use this map to adjust the agent’s behavior based on the data from the mapping process.

Secondary, there are several other outputs described in detail in IV section. We are talking about the things like exporting the 3D model of all the places that agent has visited during the mapping session, projecting neural network’s detection from RGB camera to thermal and to generating the annotated IR dataset for object detection in this way, extending existing camera images by the depth map generated from the aggregated point cloud model.

### D. Configuration

The program at the startup reads the configuration from the dedicated configuration file that keeps all the information, like the path to the offline recorded data, parametrization of the run-time algorithms, sensor calibration data files, or the logging arguments. The entire configuration is stored in the YAML format, so it is easily readable for humans and machines as well.

## III. MODULES

We have divided the project’s structure into several modules that each covers a different part of the tasks that our framework handles.

### A. Data Loaders

As our framework is currently not working with online data, there is an interface that loads stored records and provides the loaded data ordered by their timestamps to the main pipeline.

There is a data loader for every physical sensor that reads only one data series. All these data loaders are wrapped by a central data loader that creates an interface between stored data and the main pipeline. All the data loaders have ordered the timeline of their data series. When the main pipeline is ready to accept the next data packet, the central data loader asks all the subordinates loaders for their smallest timestamp, and the data loader with the lowest timestamp will provide the data packet to the processing pipeline.

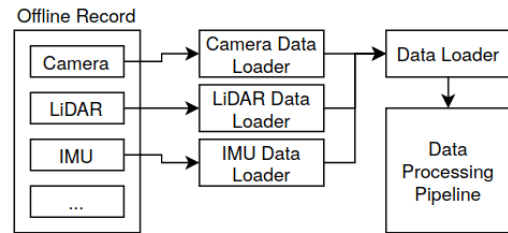


Fig. 3. Data Loader provides interface between the data processing pipeline and the sensor specific data loaders. The data are provide to the processing pipeline as a sorted data packets with respect to time.

The central data loader is providing every new data packet as a generic data type that is specified by the sensor identifier, so the main data processing pipeline can decide how to process it.

## B. Fail Check

The "Fail Check" module aggregates tools that follow the raw data from the sensors and estimates if the given sensor is reliable or not. The abstraction of this module is covered by a single class `FailChacker`, which interfaces API for the entire module. Every new data packet is passed into the instance of this class and provides this data packet into the corresponding sensor-specific fail checker. This dedicated sensor fail checker follows the data from a single sensor for the entire runtime. There could be detected anomalies, like missing data frames, empty camera frames, unreal or saturated IMU data, LiDAR data inconsistency, or any other data damage.

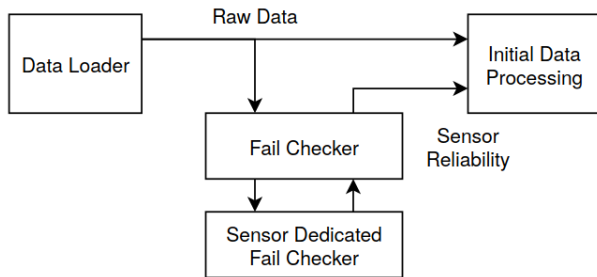


Fig. 4. Data fail checker. Every raw data packet is passed into the dedicated fail checker that tracks data reliability in the runtime and estimates sensor's reliability score.

Later the main pipeline can request the reliability of the sensor any time.

## C. Data Models

The "Data Model" section holds classes that represent the data model used internally by the processing pipelines and the input and output data.

The first part of the data models is the raw input data representation. Every sensor has one or more classes that cover the range of the input data. For example, a camera. There are two classes `CameraFrameDataModel` for RGB image representation and the `CameraIRFrameDataModel` for the thermal camera image data entity. Every instance of those classes is defined by the camera sensor identifier, precise timestamp, image frame, and optionally pre-generated YOLO neural network object detections. This data packet keeps all the important information, and the data loader passes the instance of this class when the main processing pipeline requests the latest image data.

The second part of the data models are the internal data representation models, that are used for the communication between the modules in the primary data processing pipeline, like `LidarDetection` for objects detected in the LiDAR domain, `LocalPosition` as a relative metric position w.r.t. origin of the mapping session, `FrustumDetection` for the camera-based detected objects and many others.

## D. Algorithms

the "Algorithms" module is the core one. It contains all the data processing code. There are organized classes that

cover the agent's position filtration based on the GNSS and IMU Kalman filter data fusion, functionality to projecting objects from the 3D environment into the camera frames and back, generating a depth map from the LiDAR data, or the redundant data filtration. The "Algorithms" module is the main section where the implementation of the pipelines described in section IV.

## E. Local Map

The "Local Map" module primarily represents the part of the software that holds the internal map of the surrounding environment. There are two main classes. The first one is `LocalMap`. This class is a simple container that allows us to store and read out data models of the map representation entities, like aggregated LiDAR model of the near surrounding, detected obstacles, YOLO detections, and higher representations of the more complex fused data. The second class is `ObjectsAggregator`. This class fuses low complexity detections, for example, LiDAR and camera-based detected objects into the higher complexity representation, that fuses geometrical shape information, object type, kinematic model, motion history, etc.

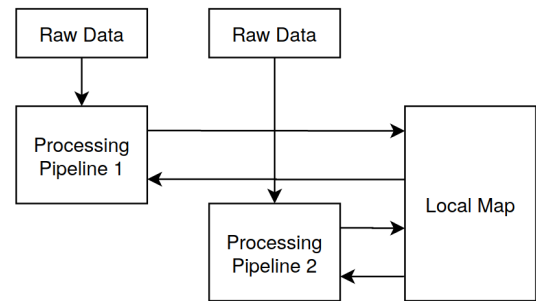


Fig. 5. Local Map works as a container for the information of the local environment extracted from the input data. All these data together create the map of the surrounding. The second part of the local map is the set of algorithms that fuses extracted information into the more complex detections.

The data stored in the Local Map are the real output of the entire framework.

## F. Visualizers

This module handles the interface between the main pipeline and the rendering engine. The main class, called `VisualizationHandler` provides a wrapper over the entire rendering logic. For every specific data type (IMU data - `ImuVisualizer`, camera frames - `CameraVisualizer`, point clouds - `LidarVisualizer`, etc.) there is dedicated class that manages the interface between the central point and the visualization engine (RViz in our case).

## G. Data Writers

Data Writer section covers the classes that are responsible for the writing Local Map data to the local hard drive storage. Currently, there are the implementations for the saving the aggregated LiDAR point cloud projected to the camera plain (see IV-E) and the class for storing RGB YOLO detections projected into the thermal camera (see IV-D).

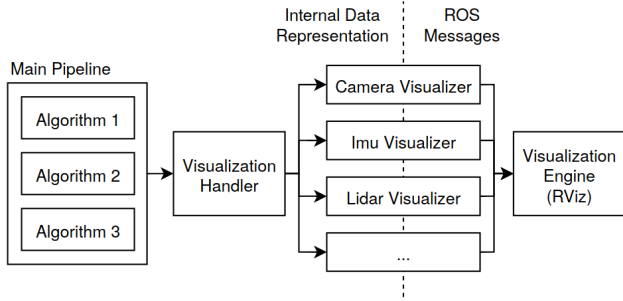


Fig. 6. Visualization scheme. From the main pipeline the internal representation data are passed into the `VisualizationHandler`. There they are switched into the specific visualization class, which manages the visualization in the rendering engine.

#### IV. DATA PROCESSING PIPELINES

The framework implements several principles of data processing and map building. In this section, we are describing the basics of the most important ones.

##### A. Precise Positioning

The most important task to deal with during the mapping process is an exact positioning. Without this functionality, there would be impossible to build up a reliable map model and to aggregate information in time.

For our purpose, we have used the differential RTK GNSS that samples a global position with the precision of one  $\sigma$  below 2cm and also provides azimuth of the measurement setup. To improve the dynamic positioning, we are also using the data of the linear acceleration and angular velocity from the IMU sensor. The example of the fusion of these sensors could be [5].

Summing it all together, the pipeline has the following input data, the global position and heading from the GNSS receiver and the linear acceleration, angular velocity, and filtered absolute orientation from the IMU sensor. The IMU automatically compensates the roll and pitch drift by the direction of the gravity, and the yaw drift compensates by the magnetic field measurement.

At the very beginning, the first GNSS position sets up an anchor that defines the origin of the mapping session. This first global position is the origin (the anchor) of the local coordinate system. The core of the position estimation process is the set of 1D Kalman filters [6], [7], that model position and speed in all three axes of the given environment. Every new incoming GNSS position is converted to the local coordinate system w.r.t. the anchor. This local position is used as a correction for the Kalman filters [8] in all three axes.

At the same time, there are incoming IMU data at several times higher frequency. For every linear acceleration data packet, it is necessary to remove the gravitation to operate only with the dynamic acceleration. For this purpose, the system models the absolute IMU orientation that is initialized by the roll and pitch angles provided by the inertial unit itself. The yaw is estimated differently. The orientation allows

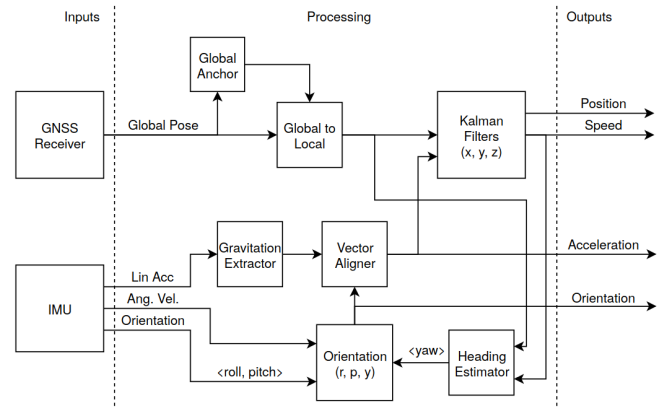


Fig. 7. Scheme of the position estimation pipeline.

us to subtract the 9.81 constant from the measured linear acceleration, and this gravitation free acceleration could be aligned with the local coordinate system and used as a prediction data for the positioning Kalman filter.

As the system models the IMU orientation separately on the IMU's internal model, for every new angular velocity data system updates its internal model to have a fast response. However, there is always a long term drift for this long-term noisy data integration. To remove the roll and pitch drifts systems fuses its internal model with the IMU's one by the low pass filter. To system to compensate the yaw drift, it combines the heading measured by the GNSS receiver and its differential antennas with the heading estimated by the speed of the agent, which is estimated by the motion model. Heading measured by the GNSS is stable, but continually contains the noise with an amplitude of about 3 degrees. During the worse signal receive conditions heading could be even lost. On the other hand, speed is direction is reliable if the agent is in motion and moves with the speed of a few meters per second. The faster the agent moves, the more system relies on the velocity vector and less on a GNSS heading. In the case of losing, the GNSS signal and low-velocity system can keep the right yaw orientation for several dozens of seconds only by the angular velocity information.

##### B. LiDAR data aggregation

As we are using the rotating 3D LiDARs, the scanners are performing measurements in different directions at different times during the scanner rotation, and the robot is constantly changing position. All these effects cause the outcome measurement to be significantly distorted. To better explain this issue, let us imagine that there is an obstacle in the very front of the LiDAR. The scanner takes several samples from this direction and then rotates clockwise to the right. As it continues to scanning full 360 degrees all around the car, at the end of the scanning LiDAR, it will direct once again in the same spot as it was at the beginning and scans once again the same obstacle. However, let us say that the agent is moving forward by the  $10\text{ms}^{-1}$  ( $36\text{kmh}^{-1}$ ). As the single scan takes 100ms, it means that the distance measurement of

the same obstacle at the beginning and the end of the scan differs by 1m. The rotation of the agent would cause an even more significant distortion effect [9], [10].

Because of this, we can not only merge all the scans into the single one, because the result would be inaccurate and blurred.

The input LiDAR data could come from several LiDAR scanners. The entire process assumes that each scan stores the data in the same order as it was measured. The input data, however, are at the beginning filtered by the data model's callback and downsampled by the `PointCloudProcessor` call instance to reduce the computational complexity of the later point cloud transformation. At the same time, the positioning system provides the agent's position at the moment in which the current and the previous scans have been taken.

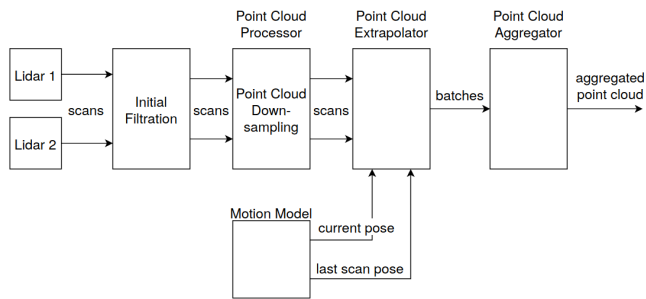


Fig. 8. Schematic of the point cloud aggregation pipeline. The input data are filtered from redundant points, downsampled to reduce the computational complexity. At the same time, the current agent's position, and the position for the previous scan is taken from history. The `PointCloudExtrapolator` splits the entire scan into the smaller batches, and for every batch is calculates linearly interpolated transformation that is proportional to the when the point has been scanned. Finally, all the bathes are aggregated in the `PointCloudAggregator`

All these three information, the scan and both positions are passed to the `PointCloudExtrapolator` instance. There the point cloud is split linearly into the  $N$  batches of the same size. Because the scan data are sorted, each batch covers a small angular section of the entire scan, which corresponds to the small-time period when the data from this batch has been taken.

For every batch, we have already estimated the transformation that is valid for a short period of time when the batch's data has been scanned. This transformation is corresponding to the IMU position w.r.t. the origin of the local coordinate system. Because of this, we have to aggregate one more transformation, the one that expresses the frame difference between the given LiDAR sensor and the IMU reference frame. In this way, we can calculate the final homogeneous transformation transform every single point cloud measurement form the scanner's frame to the local coordinates frame. However, transforming every single point is very demanding on computational power. The points are not transformed immediately, but the batch holds the data in the original frame, and the transformation could be evaluated later in the pipeline, or even more, the transformation could be aggregated for e specific purpose, and the points could be

transformed at once.

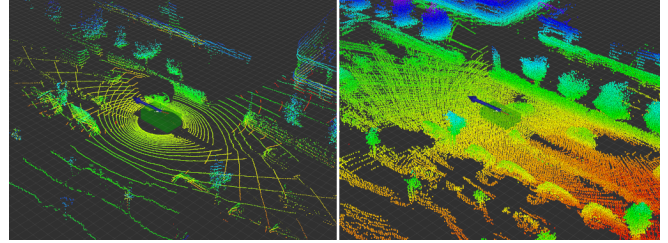


Fig. 9. Comparison of the non-aggregated point cloud from two Velodyne HDL-32e scanners (left) and the aggregated ones (right) on the aggregation period of 1.5s.

At the very end of the process, all the newly created batches are passed into the `PointCloudAggregator` class, which aggregates all the batches in time and periodically removes the old ones form the memory. This way, `PointCloudAggregator` contains the more precise and nearly undistorted model of the environment, that aggregates all the LiDAR scans from the past of the defined length.

### C. Camera-LiDAR Object Detection

LiDAR is able to measure the distance and the geometrical shape of the obstacle with high accuracy. On the other hand, to be able to recognize the specific class of the object-based only on the point cloud and geometrical shapes is quite challenging. The very opposite of this approach is an object detection on the camera images. These days neural networks are able to localize and classify objects on the RGB images in real-time with several dozens of fps [11]. However, although we have quite a reliable object classification and localization in the 2D plane, it is tough to estimate the distance of the detected object.

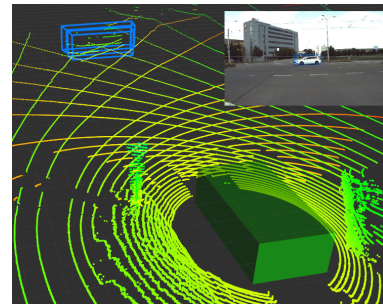


Fig. 10. Car detected by the neural network in both frontal cameras. Distance of the 2D detection is estimated based on the aggregated LiDAR data. Camera view in the right top corner.

For this purpose, we have created a system that combines the LiDAR data and camera detections and combines them into a single representation.

For every detection on the RGB image, there is an estimated median distance of the LiDAR measurements that have been projected to the detection bounding box and, based on this information system, generated the 3D frustum representation in the output map of the detected obstacle. The frustum begins in the optical center of the camera and

points to the middle of the 2D detection bounding box. The distance measured by the LiDAR defines the cutout of the frustum in which the obstacle is present.

#### D. RGB YOLO Detections to IR Image

If we focus on the field of neural network training, we can find a large number of papers [12], [13], [14] that deal with object detection on the RGB images. However, much fewer works are focusing on thermal images [15]. Even so, the thermal domain is very beneficial for the autonomous agents because it allows agents to sense the surroundings even in the wrong lighting or weather conditions.

There is not only a smaller number of works that are interested in the learning neural networks to detect objects on the thermal images [16], [17] compared to the visible light spectrum, but also there is also a dramatically smaller background in existing datasets. There are very few publicly available sources of annotated thermal images that could be used for training purposes, like KAITS [18] or the FLIR [19].

Because of this, we have proposed the system that would be able to automatically generate a large amount of annotated IR images based on the transferring object detections from the RGB images to the thermal ones, which will help in the future when we will train neural networks for in the thermal image domain [20].

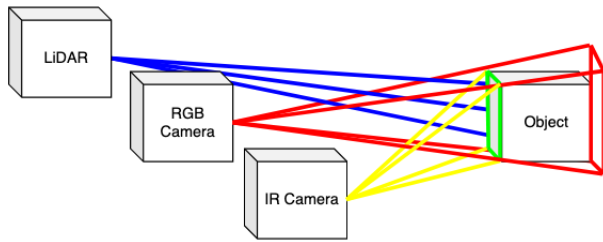


Fig. 11. 1 (red) - the YOLO neural network detects objects in the RGB image. This 2D detection can be represented as a 3D frustum in the real world. 2 (blue) - the LiDAR measures object distance. 3 (green) - by combining LiDAR data and 3D frustum, we can estimate the frontal plane of the detected object. 4 (yellow) - the detected object's plane is reprojected into the IR camera.

The basic idea is to preprocess the detections on the RGB camera, which is physically very close to the IR camera and is also oriented in the same direction. For every RGB frame for which the object detection has been performed, the nearest IR frame in time has been chosen. In the next phase, the aggregated point cloud model (see IV-E) is used to estimate the distance of the detected obstacle so that the obstacle can be transformed from the 2D image plane into the 3D model of the environment. The last phase is to project the frontal phase of the 3D modeled obstacle into the thermal image, as shown on the fig. 12 and store the parameters of the projected objects in the same format as the origin RGB detections do.

#### E. Aggregated LiDAR Data to Image Projection

As we have created the system described in the IV-B, which undistorts and aggregates LiDAR data into the single



Fig. 12. An example of the RGB detections mapped onto the thermal camera using the distance estimate from time-integrated LiDAR scans.

point cloud model, we have found very useful to use these data in the field of neural network training.

Currently, there is a huge number of academical publication that deal with the convolutional neural networks, and how to improve the performance of those state-of-the-art algorithms. However, there is a large number of papers that cover the RGB image object detection, but much less of those that would be dealing with the object classification and detection in the IR (thermal) domain [21] and even less that would try to process the depth images [22].

Our project allows us to merge all these three domains into a single problem. Our research is focusing on joining the RGB, IR, and depth images into the single multi-domain picture, which could potentially improve the neural network's understanding of the scene.

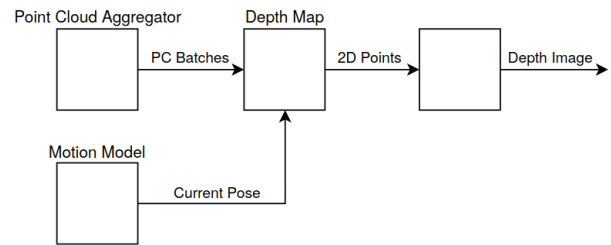


Fig. 13. Schematic of the depth image generation.

Every new frame from the thermal camera triggers the following process. From the motion model, there is requested the current position of the IMU in the local coordinate system. At the same time, the transformation between the IMU and the IR camera is known from the calibration frame.

From the `PointCloudAggregator`, the currently aggregated set of the point cloud batches is requested and passed into the instance of the `DepthMap` class. The `DepthMap` is also provided by the current position and the IMU to camera transformation and the camera calibration parameters. By combining all this information, for every point cloud batch, there is applied additional transformation, so currently, the entire transformation chain is following from LiDAR frame to IMU frame to the Origin frame to the IMU frame to the IR Camera frame. Still, every point is transformed only once, because the transformation has been chained and lazy performed. Now the `DepthMap` can project transformed points into the camera chip plain, so the 3D points are converted to 2D coordinates, and all points that

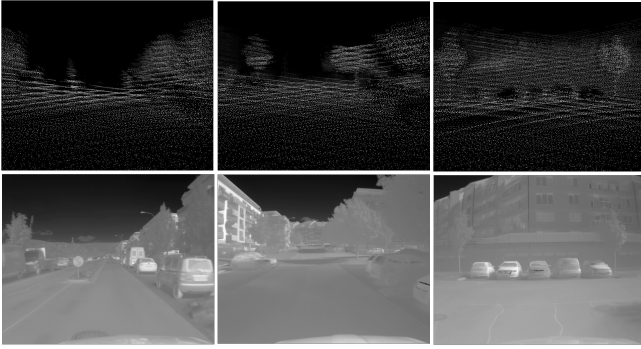


Fig. 14. Example of depth images generated based on the aggregated point cloud model. Depth images (top) paired with the corresponding thermal images (bottom). Point cloud has been projected to the camera frame. The same technique can be applied also on RGB images.

lie behind the image borders are removed. On the very end, all the 2D points are plotted into the blank image, and the image is stored with the sequence number of the original incoming IR frame.

#### F. Visualizations

The entire mapping process requires a detailed visualization backend to correctly understand every step of the data processing as well as the final output environment model. For this purpose, we have used RViz - the visualization tool of the ROS toolkit. It supports elementary geometry object like points of lines as well as more complex shapes, like arrows, polylines, and also complex visualizations, like point clouds, occupancy grids, or the transformation trees.

During the mapping process, RViz visualizes raw data from every single sensor, both LiDARs, all the cameras, IMU, and the GNSS receiver. To better understand the mapping process there are the visualizations of the position history, merged and undistorted point cloud from both LiDARs, objects detected in the LiDAR data, objects detected by YOLO neural network at the RGB images, current speed and position modeled by the positioning system, filtered linear acceleration and many more.

A handy feature is that RViz can project the entire rendered 3D scene into the image stream, so we can easily validate the matching of the camera-LiDAR calibration.

In the case that someone would like to migrate on the other visualization platform, there is no need to make any significant modifications. The `VisualizationHandler` encapsulates the entire visualization. This class creates an interface between the mapping framework and the backend that communicates with the rendering engine. If someone would decide, do migrate on the different visualization system, it needs to modify this backend, and the API of the `VisualizationHandler` stays the same so that the eventual modification would have no impact on mapping code.

## V. EXTERNAL DEPENDENCES

Most of the problems that we have to deal with during the time we are creating something new are the problems

that have already been solved before by someone else. The same is true for our framework. We have used several public projects that helped us to define standards that our system uses for data communication and data storage, raw data representations, like 3D vectors or the rotation angles.

#### A. Robotic Operating System

ROS [23] is, by these days, the more or less standard for non-real-time solutions in the field of robotics. This library has defined the way how real deployed projects are managing data transportation and storage or the scaling system into the multi-agent form.

We have primarily used ROS for data storage and visualizations. As we have recorded a large amount of data during the Brno Urban Dataset[3] creation, we have stored all the recorded data in the format that is fully compatible with common ROS messages. In this way, there anybody uses the data in the own way, and ROS message standards that are used by large community guaranties that we did not miss any critical information from the raw sensor output.

The second primary purpose is to use the ROS visualizations. ROS provides a handy tool for 3D visualizations called RViz. This program can listen to the standard ROS messages and convert them into simple 3D graphics that help to understand the inner processes inside the data processing algorithms.

As the work on our project begins in 2018, we have decided to use the first version on the ROS. By these days, it would be possible to move dependencies to ROS2, which provides more advanced network communication or the support or the real-time applications.

#### B. Robotic Template Library

For the underlying data representation, like N-dimensional vectors, rotation angles, and matrices, quaternions, bounding boxes, frustums, transformations, etc., we have used the previous work of one of the authors.

RTL builds on Standard Template Library (STL) of the C++17 language and the Eigen library for highly optimized linear algebra and related tasks. An original purpose of RTL was to put together an experimentation toolkit for research in robotic mapping and localization, however over the years, it became a little more mature, and it seemed worthwhile to be offered to the community on <https://github.com/Robotics-BUT/Robotic-Template-Library>. Next to the fundamental data primitives representation, RTL also provides several algorithms for point cloud segmentation and vectorization [24], [25], which are used for point cloud processing in the Atlas system.

#### C. Munkres Algorithm

To simplify the assignment problem when algorithms are matching 3D detections to each other, we have used the existing project [26] available on <https://github.com/aaron-michaux/munkres-algorithm>. It is a lightweight C++17 implementation of the Munkres Algorithm with straightforward, single-function API.

## VI. FUTURE WORK

We have designed our framework in the way that the architecture allows anybody to modify or extend the existing solution. We have put a special effort into building up the an abstract system that allows us to scale the current solution to a much larger solution with a reasonable amount of additional complexity. For example, to implement the new sensor's data, there is no need to modify existing data models and data loaders. We can extend current software with a few new lines of code based on the given templates. The same we can say about the processing pipelines.

In the future, we are preparing to add more sensors, like radar or ultrasound sensors, extend current pipeline with the disparity map generation based on the two frontal cameras, optical odometry, or semantic scene segmentation by the neural networks.

We would also like to make this project fully open-source because we believe that these kinds of projects can reach a more significant number of developers and researchers, and the bigger community means a more dynamic development process. Our target is to provide a research platform for a large research community that will not need to develop many of those algorithms from scratch and will be able to improve more specific problems for the autonomous robot or the self-driving car domain.

## VII. CONCLUSION

As a result of the AutoDrive research project, we have created the experimental mapping framework that allows easy and fast prototyping of new approaches in the field of autonomous agents. We have divided the project into several modules, each with a lightweight API. The main data processing pipeline is a single thread with a waterfall-like architecture, so it makes it easy to understand the way, how the data are processed and also the modification does not require complicated code refactoring.

The essential parts of our framework are the precise positioning system that fuses GNSS and IMU data, the LiDAR scans aggregator, that allows us to integrate multiple point clouds into a single dense model of the environment. Next, there is the point cloud to camera projection and depth image generating, the point cloud obstacle detection, YOLO neural network-based 3D obstacle detection, RGB to IR neural network detection mapping.

To share our work and help other researches with their work, we are making the entire project fully open-source.

## REFERENCES

- [1] S. Kato, S. Tokunaga, Y. Maruyama, S. Maeda, M. Hirabayashi, Y. Kitsukawa, A. Monroy, T. Ando, Y. Fujii, and T. Azumi, "Autoware on board: Enabling autonomous vehicles with embedded systems," in *2018 ACM/IEEE 9th International Conference on Cyber-Physical Systems (ICCP)*. IEEE, 2018, pp. 287–296.
- [2] W. Li, C. Pan, R. Zhang, J. Ren, Y. Ma, J. Fang, F. Yan, Q. Geng, X. Huang, H. Gong *et al.*, "Aads: Augmented autonomous driving simulation using data-driven algorithms," *arXiv preprint arXiv:1901.07849*, 2019.
- [3] A. Ligocki, A. Jelinek, and L. Zalud, "Brno urban dataset—the new data for self-driving agents and mapping tasks," *arXiv preprint arXiv:1909.06897*, 2019.
- [4] W. Maddern, G. Pascoe, C. Linegar, and P. Newman, "1 year, 1000 km: The oxford robotcar dataset," *The International Journal of Robotics Research*, vol. 36, no. 1, pp. 3–15, 2017.
- [5] F. Caron, E. Duflos, D. Pomorski, and P. Vanheeghe, "Gps/imu data fusion using multisensor kalman filtering: introduction of contextual aspects," *Information fusion*, vol. 7, no. 2, pp. 221–230, 2006.
- [6] R. E. Kalman, "A new approach to linear filtering and prediction problems," 1960.
- [7] S. Thrun, "Probabilistic robotics," *Communications of the ACM*, vol. 45, no. 3, pp. 52–57, 2002.
- [8] G. A. Terejanu, "Discrete kalman filter tutorial," *University at Buffalo, Department of Computer Science and Engineering, NY*, vol. 14260, 2013.
- [9] P. Merriaux, Y. Dupuis, R. Boutheau, P. Vasseur, and X. Savatier, "Lidar point clouds correction acquired from a moving car based on can-bus data," *arXiv preprint arXiv:1706.05886*, 2017.
- [10] B. Zhang, X. Zhang, B. Wei, and C. Qi, "A point cloud distortion removing and mapping algorithm based on lidar and imu ukf fusion," in *2019 IEEE/ASME International Conference on Advanced Intelligent Mechatronics (AIM)*. IEEE, 2019, pp. 966–971.
- [11] A. Bochkovskiy, C.-Y. Wang, and H.-Y. M. Liao, "Yolov4: Optimal speed and accuracy of object detection," *arXiv preprint arXiv:2004.10934*, 2020.
- [12] J. Redmon and A. Farhadi, "Yolov3: An incremental improvement," *arXiv preprint arXiv:1804.02767*, 2018.
- [13] W. Liu, D. Anguelov, D. Erhan, C. Szegedy, S. Reed, C.-Y. Fu, and A. C. Berg, "Ssd: Single shot multibox detector," in *European conference on computer vision*. Springer, 2016, pp. 21–37.
- [14] Z.-Q. Zhao, P. Zheng, S.-t. Xu, and X. Wu, "Object detection with deep learning: A review," *IEEE transactions on neural networks and learning systems*, vol. 30, no. 11, pp. 3212–3232, 2019.
- [15] K. Agrawal and A. Subramanian, "Enhancing object detection in adverse conditions using thermal imaging," *arXiv preprint arXiv:1909.13551*, 2019.
- [16] M. Ivašić-Kos, M. Krišto, and M. Pobar, "Human detection in thermal imaging using yolo," in *Proceedings of the 2019 5th International Conference on Computer and Technology Applications*, 2019, pp. 20–24.
- [17] C. Herrmann, M. Ruf, and J. Beyerer, "Cnn-based thermal infrared person detection by domain adaptation," in *Autonomous Systems: Sensors, Vehicles, Security, and the Internet of Everything*, vol. 10643. International Society for Optics and Photonics, 2018, p. 1064308.
- [18] J. Jeong, Y. Cho, Y.-S. Shin, H. Roh, and A. Kim, "Complex urban dataset with multi-level sensors from highly diverse urban environments," *The International Journal of Robotics Research*, p. 0278364919843996, 2019.
- [19] Tech. Rep., also available as <https://www.flir.in/oem/adas/adas-dataset-form/>.
- [20] L. Y. Pratt, "Discriminability-based transfer between neural networks," in *Advances in neural information processing systems*, 1993, pp. 204–211.
- [21] C. D. Rodin, L. N. de Lima, F. A. de Alcantara Andrade, D. B. Haddad, T. A. Johansen, and R. Storvold, "Object classification in thermal images using convolutional neural networks for search and rescue missions with unmanned aerial systems," in *2018 International Joint Conference on Neural Networks (IJCNN)*. IEEE, 2018, pp. 1–8.
- [22] T. Ophoff, K. Van Beeck, and T. Goedemé, "Exploring rgb+ depth fusion for real-time object detection," *Sensors*, vol. 19, no. 4, p. 866, 2019.
- [23] M. Quigley, K. Conley, B. Gerkey, J. Faust, T. Foote, J. Leibs, R. Wheeler, and A. Y. Ng, "Ros: an open-source robot operating system," in *ICRA workshop on open source software*, vol. 3, no. 3.2. Kobe, Japan, 2009, p. 5.
- [24] A. Jelinek, L. Zalud, and T. Jilek, "Fast total least squares vectorization," *J. Real-Time Image Process.*, vol. 16, no. 2, p. 459–475, Apr. 2019.
- [25] A. Jelinek and L. Zalud, "Augmented postprocessing of the ftls vectorization algorithm," in *Proceedings of the 13th International Conference on Informatics in Control, Automation and Robotics*, ser. ICINCO 2016. Setubal, PRT: SCITEPRESS - Science and Technology Publications, Lda, 2016, p. 216–223.
- [26] R. Pilgrim, "Tutorial on implementation of munkres' assignment algorithm," 08 1995, p. 13.